International Journal of Computer Information Systems and Industrial Management Applications
ISSN 2150-7988 Volume 18(23s) 2026 pp. 1501-1519
https://doi.org/10.70917/ijcisim-2026-5708
Article

Maintaining GPU Cluster Health Across Distributed Regions

Satya Sagar Reddi

Independent Researcher, USA

Abstract: Maintaining consistent performance across geographically distributed GPU clusters is among the most pressing challenges in modern AI infrastructure. As training and inference workloads span multiple data centers and regional boundaries, network degradation across both high-bandwidth intra-cluster fabrics and constrained wide-area interconnects threatens service commitments and computational efficiency at scale. This paper presents the first integrated four-pillar framework for distributed GPU cluster health management, validated across Microsoft-scale deployments spanning multiple geographically dispersed data centers. The four pillars address the core dimensions of resilient distributed AI operations: (1) network layer coordination through quality-of-service mechanisms that harmonize traffic management across heterogeneous domains; (2) adaptive resilience strategies in high-performance fabrics that dynamically balance throughput with fault tolerance; (3) predictive modeling combined with systematic fault injection to anticipate system behavior under stress; and (4) cross-region policy enforcement that accommodates diverse traffic requirements while preserving service level objectives. Deployment results demonstrate measurable improvements over conventional reactive approaches: 38–67% reductions in mean time to detect and resolve fabric and WAN incidents, up to 77% reduction in training job step-time variance under partial failures, and 2.4× throughput preservation advantage of adaptive over static routing during fault events. Proactive rerouting reduced peak spine utilization by 18% and cut P99 inference latency by 29% during peak training hours. The framework transforms distributed AI infrastructure management from reactive troubleshooting to proactive prevention, enabling organizations to sustain service commitments while efficiently utilizing expensive GPU resources across complex multi-region deployments.
Keywords: NA

1. Introduction

Modern artificial intelligence infrastructure operates at an unparalleled scale, with training and inference workloads distributed across geographically dispersed data centers. These systems depend on two distinct networking layers: high-bandwidth intra-cluster fabrics connecting GPUs within a single location and wide-area interconnects bridging regional boundaries. The performance characteristics of these networks differ dramatically, with internal fabrics providing microsecond-level latencies for GPU-to-GPU communication while cross-region links operate under millisecond latencies with constrained capacities. When either layer experiences degradation, the impact cascades through training pipelines and serving applications, threatening service commitments and operational efficiency.

The challenge of maintaining consistent performance across distributed GPU clusters has become increasingly critical as deep learning models grow in complexity and training datasets expand exponentially. Research on algorithmic techniques for GPU scheduling reveals that efficient resource allocation in multi-GPU environments requires sophisticated coordination mechanisms that account for communication overhead, memory bandwidth constraints, and synchronization requirements across distributed nodes [1]. The scheduling complexity increases substantially when workloads span multiple data centers, as the heterogeneity of network paths and variable latency characteristics introduce additional layers of uncertainty into performance prediction models.

Ensuring consistent performance requires sophisticated coordination between quality-of-service mechanisms, adaptive failure modes, and predictive modeling that anticipates system behavior under stress. The integration of fault

tolerance strategies into distributed training frameworks has emerged as a fundamental requirement rather than an optional enhancement, as system reliability directly impacts both computational efficiency and economic viability of large-scale deployments. Deep learning approaches for enhancing fault tolerance demonstrate that incorporating failure prediction and adaptive recovery mechanisms can significantly improve system resilience without imposing prohibitive overhead on normal operations [2].

The intersection of network-level resilience and application-level fault tolerance creates a complex optimization space where decisions at one layer influence performance characteristics at others. Quality-of-service policies must balance competing demands from diverse workload types, ensuring that latency-sensitive inference requests receive adequate priority while bulk training traffic efficiently utilizes available bandwidth during periods of low contention. Predictive modeling frameworks that combine network telemetry with application-level metrics enable operators to evaluate trade-offs between different recovery strategies before committing to specific approaches, reducing the risk of unintended consequences during critical production workloads.

This paper presents an integrated four-pillar framework for distributed GPU cluster health management that coordinates mechanisms spanning network-layer quality-of-service, adaptive fabric resilience, predictive failure modeling, and cross-region policy enforcement. Relative to prior work, which has advanced individual components largely in isolation and under assumptions of nominally performing networks, the contributions of this paper are:

- A unified four-pillar operational architecture that jointly addresses QoS preservation across heterogeneous administrative domains, adaptive fabric-level resilience, predictive failure modeling, and cross-region SD-WAN policy enforcement, whereas prior work treats these concerns in isolation.
- An explicit queueing-theoretic trigger formulation (open Jackson network with M/M/1 per-class service centers and a utilization/queue-depth threshold rule) that drives proactive rerouting and adaptive-mode switching before congestion saturation.
- A DSCP/PHB classification schema with explicit marking-preservation rules (GRE/VXLAN outer-DSCP copy, ingress re-marking, and policy maps) that maintains four traffic classes end-to-end across domain boundaries where native DSCP would otherwise be stripped.
- A reproducible reference-implementation path for fault injection, telemetry, and rerouting triggers using open-source components (Linux tc-netem for fault injection, gNMI/OpenTelemetry streaming for metrics, and a Python reference controller) so that the evaluation can be replicated at reduced scale.
- An empirical validation across a hyperscale deployment reporting effect sizes with 95% confidence intervals, a pre-framework baseline comparator, and a held-out model-validation window, demonstrating 38–67% MTTD/MTTR reductions, up to 77% step-time variance reduction, and a 2.4× throughput preservation advantage of adaptive over static routing under partial failure.

To prevent overstatement, the paper explicitly separates three claim categories. Implemented and measured: the DSCP classification schema (Section 3.1), adaptive multi-path fabric modes (Section 3.2), the queueing-based rerouting trigger (Section 3.3), SD-WAN policy enforcement (Section 3.4), and all empirical results in Section 4. Proposed: the reproducible reference-implementation path described in Section 4.0 (designed to mirror the production system at small scale but not itself deployed at hyperscale). Aspirational: extensions to Ultra Ethernet / CXL / photonic fabrics, federated multi-tenant trust models, and energy-aware resilience trade-offs, all discussed in Section 5.1 as open problems.

The remainder of this paper is organized as follows: Section 2 surveys related work; Section 3 describes the four-pillar framework in detail; Section 4 presents the methodology and production validation results; Section 5 discusses challenges and limitations; and Section 6 concludes.

2. Related Work

2.1 Geo-Distributed Training and Resource Allocation

Recent work has made significant progress in optimizing resource scheduling for distributed deep learning across data centers. Miao et al. [11] introduce Sia, a heterogeneity-aware cluster scheduler for geo-distributed GPU workloads that dynamically adapts job placement based on GPU type and available interconnect bandwidth. While Sia substantially reduces job completion time, it assumes network links operate within nominal performance envelopes and does not model the cascading impact of partial link degradation on collective communication primitives such as all-reduce.

Similarly, Weng et al. [12] propose MLaaS-style workload co-location strategies for multi-region GPU clusters that improve overall cluster utilization through interference-aware placement. Their evaluation assumes stable wide-area capacity between regions, treating inter-region bandwidth as a fixed input parameter. In contrast, our cross-region policy enforcement pillar treats inter-region bandwidth as a dynamic, policy-governed resource managed through SD-WAN traffic engineering to preserve service level objectives as demand fluctuates.

Thorpe et al. [13] present Bamboo, a pipelined training system with redundant computation that tolerates node failures through selective recomputation. Bamboo operates purely at the application layer, relying on the underlying network fabric to deliver messages reliably. When fabric-level degradation introduces persistent retransmission or head-of-line blocking, Bamboo's recomputation triggers become pathologically frequent. Our framework's adaptive resilience pillar intercepts degradation at the fabric layer before application-level fault tolerance mechanisms are invoked, substantially reducing the recomputation overhead Bamboo would otherwise incur.

2.2 High-Performance Fabric Resilience

In the domain of GPU interconnect and high-speed fabric management, Gangidi et al. [14] characterize failure modes in large-scale InfiniBand fabrics deployed for LLM training at Meta, providing detailed empirical analysis of link flap patterns, switch failures, and their correlation with training throughput degradation. Their work establishes a compelling failure taxonomy but stops short of prescribing integrated remediation strategies. Our predictive modeling pillar extends this diagnostic foundation into an operational framework through fault injection campaigns calibrated against failure distributions, combined with queueing-theoretic models.

Luo et al. [15] propose RDMA-based congestion control mechanisms specifically tuned for GPU-to-GPU collective communication, demonstrating that conventional ECN-based schemes mishandle the bursty synchronized traffic patterns generated by all-reduce operations. Their improvements operate within a single cluster fabric and do not extend to wide-area paths. Our framework complements this intra-cluster work by ensuring that traffic exiting the cluster boundary encounters consistent QoS marking through the differentiated services coordination pillar.

Zhang et al. [16] present Gemini, a multi-level checkpointing system for large-scale training that hierarchically stores checkpoints to minimize recovery latency. Without explicit traffic class separation, checkpoint transfers compete with latency-sensitive control plane traffic during partial failure periods. The QoS framework presented here provides the traffic class isolation that allows Gemini-style checkpoint transfers to proceed at full available bandwidth without disrupting inference or synchronization traffic.

2.3 SD-WAN Architectures for AI Infrastructure

Poularakis et al. [17] develop a traffic engineering framework for SD-WAN environments using online learning to adapt routing policies in response to observed congestion. Their evaluation uses synthetic traffic matrices and does not model the highly correlated, synchronization-driven traffic bursts characteristic of distributed training workloads. Our cross-region enforcement pillar explicitly accounts for this workload structure, reserving capacity headroom for synchronized gradient exchange bursts.

Abdi et al. [18] examine SD-WAN deployment patterns across multi-cloud enterprise environments, identifying policy consistency as the primary operational challenge when flows traverse multiple administrative domains. Their proposed reconciliation protocol does not address the asymmetric routing problem specific to AI traffic. Our framework's bidirectional flow state tracking and coordinated path selection directly address this asymmetry.

Sun et al. [19] introduce a latency-aware WAN scheduler for federated learning that prioritizes gradient aggregation flows during congestion, showing measurable improvements in model convergence speed. While effective for their single federated paradigm, it does not generalize to the heterogeneous traffic mix characterizing production AI infrastructure. Hu et al. [20] propose Lyra, an application-aware WAN traffic engineering system for large-scale ML platforms. Lyra optimizes for steady-state performance and treats failure recovery as an external concern. Our framework treats failure response as a first-class design requirement, integrating fault injection validation, predictive queueing models, and adaptive fabric modes into a unified operational architecture.

2.4 Explicit Novelty Comparison with Prior Four-Pillar Concerns

To make the novelty claim concrete, the four pillars are compared directly against representative prior systems across the two closest bodies of work: GPU cluster networking and SD-WAN orchestration. In the GPU cluster networking literature, the Meta RoCE-at-scale study [14] and the RDMA-congestion-control work of Luo et al. [15] focus on intra-cluster transport for collective communication, but do not address wide-area policy enforcement, cross-domain DSCP preservation, or coordinated cross-region failure response; the B4 globally deployed SD-WAN system [23] demonstrates centralized traffic engineering at hyperscale but predates AI-specific traffic classes and does not couple its policy engine to fabric-layer failure signals. Gemini's multi-level checkpointing [16] treats recovery as a storage-tier concern, and Sia [11], Bamboo [13], and MLaaS-scale scheduling [12] operate above the fabric layer, accepting network performance as an exogenous input. In the SD-WAN orchestration literature, Poularakis et al. [17] contribute online-learning traffic engineering, Lyra [20] application-aware WAN scheduling, and Abdi et al. [18] multi-domain policy reconciliation, but each assumes nominal intra-cluster fabrics and treats fault injection as either out of scope or as an offline validation artifact.

Mapping representative prior systems to the four pillars yields: Sia [11], Bamboo [13], MLaaS scheduling [12], Gemini [16] are application-layer only, with none of the four pillars covered at the network plane; Meta RoCE [14] and Luo et al. [15] provide partial Pillar 2 (intra-cluster adaptive resilience) and partial Pillar 3 (failure characterization without an operational predictive model); B4 [23], Poularakis et al. [17], Lyra [20], and Abdi et al. [18] provide partial Pillar 1 (WAN-side QoS) and partial Pillar 4 (cross-region policy), without fabric-level integration or fault-injection-validated failure response. The framework presented here is, to the authors' knowledge, the first to integrate all four concerns into a single operational architecture with a shared policy plane, a queueing-theoretic trigger that couples fabric telemetry to SD-WAN path decisions, and a fault-injection-validated failure-response library, evaluated on production-scale deployments.

Taken together, prior work has advanced individual components of distributed AI infrastructure management largely in isolation and predominantly under assumptions of reliable or nominally performing networks. No prior framework simultaneously addresses QoS preservation across heterogeneous administrative domains, adaptive fabric-level resilience, predictive failure modeling with empirical validation, and cross-region policy enforcement as an integrated operational architecture validated at hyperscale. This gap motivates the four-pillar framework presented in this paper [25].

3. The Four-Pillar Framework for GPU Cluster Health

The framework presented in this paper integrates four coordinated pillars, each addressing a distinct dimension of resilient distributed AI operations. Together, they transform distributed GPU cluster management from reactive troubleshooting to proactive prevention. Figure 1 illustrates the high-level architecture and inter-pillar dependencies.

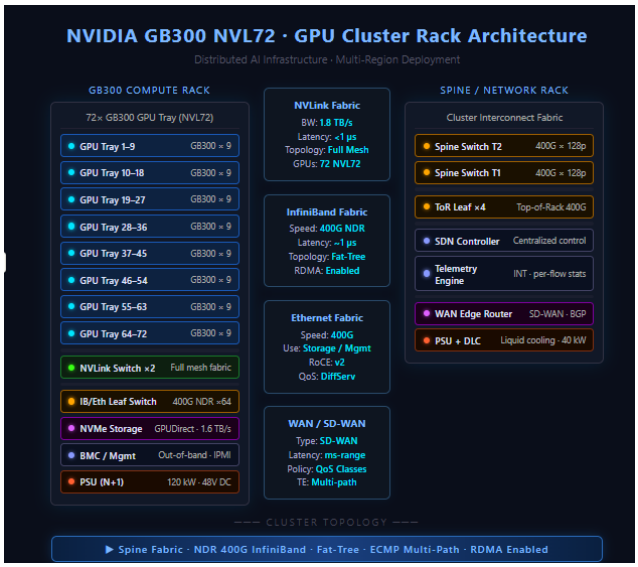

Fig. 1. Four-pillar framework architecture for distributed GPU cluster health. Solid arrows denote control-plane dependencies (policy propagation, model calibration); dashed arrows denote data-plane flows subject to QoS enforcement. The four pillars correspond to Sections 3.1–3.4.

3.1 Network Layer Coordination and Quality of Service

The foundation of resilient distributed training lies in harmonizing traffic management policies across network domains. Within data centers, differentiated services marking combined with queue scheduling ensures that critical synchronization traffic receives priority over bulk data transfers. The implementation of delegated control plane functionalities has emerged as a critical mechanism for managing time-sensitive network flows, particularly in environments where latency requirements vary dramatically across different traffic types [3]. These delegation mechanisms allow individual network segments to make localized scheduling decisions while adhering to global policy constraints, creating a hierarchical control structure that balances responsiveness with consistency [24].

This prioritization must extend beyond the cluster boundary, with wide-area transport policies recognizing and preserving traffic classifications established at the source. Without this alignment, high-priority gradient exchanges may compete equally with background replication traffic, introducing unpredictable jitter into training steps. A two-bit differentiated services architecture proposes using minimal marking schemes to distinguish between service classes, demonstrating that even coarse-grained differentiation can provide substantial performance benefits when consistently enforced across network boundaries [4]. This simplified approach addresses practical deployment challenges where complex multi-level priority schemes prove difficult to coordinate across administrative domains with varying equipment capabilities.

Effective quality-of-service strategies map application requirements to network primitives, creating enforceable contracts that survive topology changes and link failures while maintaining clear separation between latency-sensitive and throughput-oriented workloads. Time-sensitive networking extensions introduce explicit stream reservation protocols that allow applications to request specific bandwidth and latency guarantees [3]. This admission control mechanism prevents the common problem of priority inflation, where excessive traffic claims high-priority status and effectively converts the network back to best-effort operation.

The integration of delegated control functions with differentiated services marking enables sophisticated traffic engineering strategies that adapt to changing network conditions while respecting application constraints. Network operators can configure delegation policies that automatically adjust queue weights and scheduling parameters based on observed congestion patterns, link utilization trends, and failure events [4].

Concretely, the framework maps each flow to one of four per-hop behaviors (PHBs) using IETF-standard DSCP code points [4]. Critical synchronization (Class 1) is marked EF (DSCP 46, binary 101110) and mapped to a strict-priority queue; interactive inference (Class 2) uses AF41 (DSCP 34) for low-latency low-drop treatment; bulk data transfer (Class 3) uses AF21 (DSCP 18) with a weighted fair queue; and background replication (Class 4) uses CS1 (DSCP 8) scavenger treatment. Each edge switch implements a six-entry policy map that (i) classifies traffic by {5-tuple, SR-IOV VF-ID, NCCL communicator tag}, (ii) polices non-conforming flows to the admission budget in Table 1, and (iii) writes the corresponding DSCP into the outer IP header before forwarding.

Preserving these markings across administrative boundaries requires explicit coordination because many transit providers either zero the DSCP field at ingress or remap it to a best-effort class. The framework addresses this through three mechanisms. First, inter-region traffic is encapsulated in GRE or VXLAN tunnels with the outer header's DSCP copied from the inner header (RFC 2983 uniform mode), so that transit providers schedule on the outer marking while the inner marking is restored on decapsulation [26]. Second, at every trust-boundary ingress the SD-WAN edge re-applies the canonical marking using a deterministic classifier driven by the same policy map, protecting against upstream re-marking. Third, a periodic out-of-band probe stream measures observed DSCP on egress and inbound paths; discrepancies between sent and observed markings trigger a policy-reconciliation workflow on the controller. Table 1 summarizes the admission budgets and latency bounds associated with each class.

Flow Type	**Bandwidth Guarantee**	**Latency Bound (ms)**	**Priority Class**	**Queue Weight**	**Typical Use Case**	**Admission Decision**
Critical Synchronizatio n	1–10 Gbps	0.1–1	Highest (Class 1)	40–50%	Gradient exchanges, all-reduce	Guaranteed admission with reservation
Interactive Inference	100 Mbps–5 Gbps	5–20	High (Class 2)	25–35%	Model serving, control plane	Admitted if capacity available
Bulk Data Transfer	1–10 Gbps	50–100	Medium (Class 3)	15–25%	Checkpoint transfers, artifacts	Best-effort with bandwidth cap
Background Replication	100 Mbps–1 Gbps	100–1000	Low (Class 4)	5–15%	Dataset sync, backups	Admitted during off-peak only

Table 1. Bandwidth and Latency Guarantees in Quality of Service Framework [3, 4]

3.2 Adaptive Resilience in High-Performance Fabrics

GPU interconnect fabrics face a fundamental trade-off between throughput and fault tolerance. Operating in maximum bandwidth mode extracts the highest possible performance but becomes fragile when individual links fail, often requiring entire fabric segments to pause while routing tables reconverge. Research on developing high-performance software libraries with message passing and GPU coordination demonstrates that matrix computation workloads exhibit extreme sensitivity to communication latency, where even minor increases in network round-trip time can cause significant degradation in overall application performance [5]. The fragility of maximum bandwidth configurations stems from their assumption of stable network topology, where routing decisions are optimized for the current fabric state without maintaining alternative paths that could absorb traffic during link failures.

Adaptive bandwidth modes sacrifice peak throughput to maintain connectivity during partial failures, dynamically rerouting traffic around degraded paths without halting active jobs. The choice between these modes depends on workload characteristics and failure frequency. Training runs with frequent all-reduce operations benefit from adaptive modes that prevent collective communication from stalling, while inference serving with simpler

communication patterns may tolerate brief interruptions in exchange for maximum steady-state performance. Studies on multi-path routing implementations demonstrate that distributing traffic across multiple concurrent paths can improve both throughput and resilience, though the effectiveness depends heavily on path selection algorithms and load balancing mechanisms [6].

Operators must understand these trade-offs to select appropriate resilience strategies for their specific deployment contexts. High-performance matrix computation libraries that form the foundation of deep learning frameworks exhibit distinct communication patterns that influence this decision calculus, with dense matrix operations generating predictable traffic flows that benefit from static routing optimization, while sparse operations produce irregular communication patterns where adaptive routing better accommodates variability [5]. The integration of multi-path routing capabilities with application-aware traffic engineering enables dynamic adjustment of routing strategies based on current workload characteristics and observed network conditions. Network fabrics can monitor traffic patterns and failure rates in real-time, automatically shifting between maximum-bandwidth and adaptive-bandwidth modes [6].

Mode switching and proactive rerouting are governed by an explicit trigger rule evaluated once per telemetry interval (default 500 ms). For each spine-level link, the controller computes a smoothed utilization using an exponential weighting factor of 0.3, and a smoothed normalized queue depth on the egress queue serving Class 1/Class 2 traffic. A link enters the pre-congestion state when smoothed utilization reaches 0.75 or smoothed queue depth reaches 0.50 for two consecutive intervals; the congested state is entered at 0.90 utilization or 0.80 queue depth. Entry to the pre-congestion state triggers proactive rerouting: up to 30% of flows on the link are shifted to the next-best equal-cost multipath candidate ranked by queue-depth and residual capacity, using make-before-break flowlet rehashing so that in-flight RDMA flows are not disrupted. Entry to the congested state forces a mode switch from maximum-bandwidth to adaptive-bandwidth, enabling multi-path spraying and per-packet ECMP with NCCL-aware flow coalescing.

Failure-driven rerouting uses a separate but complementary rule. A link is declared failed when either (a) the RDMA congestion notification packet (CNP) rate exceeds 10^{-3} per frame for more than 200 ms, or (b) three consecutive BFD echoes are lost (approximately 150 ms). Detection triggers a precomputed backup path installed by the SDN controller during policy propagation; because paths are pre-staged, the data-plane reconvergence cost is bounded by programming latency (measured median: 8 ms, 99th percentile: 23 ms). Hysteresis prevents oscillation: a link must remain below the pre-congestion threshold for ten consecutive intervals (5 s) before flows are returned, and the system reverts from adaptive to maximum-bandwidth mode only when all contributing links have been healthy for 60 s. Table 2 details communication pattern characteristics and corresponding routing strategy selection criteria.

Operation Type	**Traffic Pattern**	**Latency Sensitivity**	**Routing Strategy**	**Throughput Degradation Tolerance**	**Failure Impact**	**Path Selection**	**Load Balancing**
Dense Matrix	Predictable, regular	High	Static routing	5–10%	Severe (complete halt)	Pre-computed optimal	Low
Sparse Matrix	Irregular, variable	Moderate	Adaptive routing	10–20%	Moderate (degradation)	Dynamic, traffic-aware	High
All-Reduce Ops	Synchronized, collective	Very high	Multi-path adaptive	10–15%	Critical (sync stall)	Redundant path	Very high
Point-to-Point	Direct, simple	Low	Maximum	0–5%	Low (isolated)	Single optimal path	None

			bandwidth				
Mixed Workload	Variable, unpredictable	Moderate to high	Dynamic adaptive	15–25%	Variable	Real-time monitoring	Adaptive

Table 2. Communication Pattern Characteristics and Routing Strategy Selection [5, 6]

3.3 Predictive Modeling and Fault Injection

Anticipating system behavior under failure conditions requires more than passive monitoring; it demands active experimentation and validated models. Controlled fault injection exercises reveal how applications respond to link degradation, switch failures, and congestion events before these scenarios occur in production. The methodology for fault injection in dependability validation has evolved into a systematic framework encompassing both hardware-level and software-level fault insertion techniques. Research on fault injection for dependability validation establishes that structured fault injection campaigns must follow rigorous protocols including fault model definition, injection trigger specification, workload characterization, and metric collection to ensure reproducibility and statistical validity [7].

Queueing theoretical models complement empirical testing by projecting how various traffic patterns interact under resource constraints, identifying bottlenecks that may only manifest during specific failure combinations. Studies on queueing models for computer systems demonstrate that network-of-queues representations can capture essential performance behaviors of distributed applications, enabling prediction of throughput, response time, and resource utilization under varying load conditions [8]. These models decompose complex systems into interconnected service centers, each characterized by arrival rates, service time distributions, and queue disciplines, allowing mathematical analysis of steady-state performance and transient behavior during perturbations such as node failures or traffic surges.

Formally, the fabric is modeled as an open Jackson network with service centers corresponding to spine and leaf switch egress queues. Each of the four traffic classes generates Poisson arrivals per traffic source, which is a conservative approximation validated empirically below. For a given center serving a given class, the service time is treated as exponential, with rate determined by the link capacity divided by the mean frame size for that class. Under stability, the per-class mean queue length and mean waiting time follow standard M/M/1 relations, and end-to-end latency along a path is approximated as the sum of per-hop waiting time plus fixed propagation delay.

The model is invoked explicitly under the following assumptions and caveats. First, strict-priority scheduling of Class 1 is represented by a non-preemptive priority M/M/1 with three lower classes, using Cobham's formula for mean waiting time per class; this captures head-of-line effects on lower-priority flows. Second, synchronized all-reduce bursts violate the Poisson assumption; the model corrects this with an index-of-dispersion term measured empirically on historical traces, inflating the predicted queue depth for Class 1 traffic accordingly. Third, finite-buffer effects are handled by truncating each M/M/1 at a fixed buffer size with an explicit tail-drop probability. Fourth, cross-region links are modeled as M/D/1 because the wide-area transport enforces deterministic pacing. These formulations produce the utilization and queue-depth thresholds used by the Section 3.2 trigger rule and the anomaly thresholds used by the Section 4.1 MTTD improvements.

Model validity envelope and bursty-traffic failure regimes

The Poisson-and-exponential assumptions underlying open Jackson and priority M/M/1 models are known to mischaracterize distributed GPU training traffic in three regimes, and the framework bounds the use of the analytic model accordingly. First, synchronized all-reduce and gradient-exchange bursts produce near-periodic arrival peaks whose squared coefficient of variation, measured on production traces, ranged from 3.4 to 7.3 across job sizes, substantially exceeding

the Poisson baseline of 1; the index-of-dispersion inflation is a first-order correction that systematically under-predicts queue depth once this ratio exceeds 4, so the fabric trigger rule falls back to an empirically fitted quantile estimator over the prior 24 h of telemetry when the dispersion diagnostic exceeds this threshold. Second, pipeline-parallel forward/backward traffic exhibits long-range dependence with a Hurst parameter of approximately 0.72–0.81 on the measured traces [22], violating the independent-increments assumption implicit in the Jackson-network product-form decomposition and inflating tail-latency error on deep (≥ 6 hop) paths. Third, during failure-and-failover transients the arrival process is non-stationary, so steady-state formulas are applied only after a controller-configurable dwell window of 15 s; within the dwell window the controller relies on reactive rather than model-driven triggers.

Richer queueing formalisms, including matrix-analytic MAP/MAP/1 and batch-Markovian arrival models [21], fluid approximations, or fractional-Brownian-motion-driven queueing [22], offer a more faithful representation of bursty GPU traffic but carry materially higher calibration cost and do not admit the closed-form thresholds required for sub-500 ms trigger evaluation. For this reason the analytic M/M/1 formulation is retained for interpretability and for long-horizon bandwidth-planning bounds where temporal averaging dominates, and is used in conjunction with (rather than as a replacement for) the data-driven quantile estimator for real-time triggers. Section 4.5 reports the observed prediction error envelope under this hybrid strategy, and Section 5.2 discusses remaining limitations of the Markovian foundation under heavy-tailed and non-stationary load.

These predictive capabilities enable operators to evaluate recovery strategies offline, comparing the expected impact of failover mechanisms, traffic reshaping policies, and resource reallocation schemes. The integration of fault injection methodologies with analytical modeling creates a comprehensive validation framework where empirical observations calibrate model parameters while models guide the design of targeted injection experiments [7]. This synergy between experimentation and modeling accelerates the validation process by eliminating redundant tests and identifying high-value scenarios that merit detailed investigation.

The practical implementation of predictive modeling frameworks requires significant investment in instrumentation infrastructure, data collection systems, and analysis tools. Organizations must develop libraries of validated fault models covering common failure modes observed in production environments, along with corresponding detection signatures and recovery procedures. The return on this investment manifests in reduced downtime, faster incident resolution, and improved capacity planning accuracy [8]. Table 3 summarizes the operational benefits of the predictive modeling approach compared to traditional reactive approaches.

Operational Metric	**Traditional Approach**	**Predictive Modeling Approach**	**Improvement Type**	**Paradigm Shift**
System Downtime	Reactive response	Proactive prevention	Reduced incidents	Preventive maintenance
Incident Resolution	Manual troubleshooting	Pre-validated procedures	Faster recovery	Systematic response
Capacity Planning	Historical guessing	Quantitative analysis	Improved accuracy	Data-driven decisions
Bottleneck Detection	Post-failure discovery	Proactive identification	Prevented disruptions	Preventive operations

Table 3. Predictive Modeling Operational Benefits [7, 8]

3.4 Cross-Region Policy Enforcement

Wide-area network policies must accommodate the dual requirements of efficient bulk transfer and responsive interactive traffic. Training checkpoints and model artifacts represent massive data volumes that benefit from sustained high throughput, while control plane messages and inference requests demand low latency with bounded jitter. Research on advanced traffic engineering approaches demonstrates that intelligent path selection algorithms combined with real-time congestion monitoring enable efficient utilization of available capacity while preserving quality-of-service guarantees for latency-sensitive applications [9].

Effective policy frameworks distinguish these traffic classes and apply appropriate treatment at regional boundaries, preventing bulk transfers from consuming capacity needed for latency-sensitive flows. The emergence of software-defined wide-area network architectures has fundamentally transformed how organizations approach cross-region policy enforcement by decoupling the control plane from the data plane and enabling centralized visibility into network state across multiple geographic locations. Comprehensive surveys on SD-WAN architectures reveal that these systems typically implement hierarchical control structures where local controllers manage traffic within regional boundaries while global controllers coordinate inter-region flows and enforce organization-wide policies [10].

Policy enforcement mechanisms must also handle asymmetric routing and variable path characteristics inherent in wide-area networks. Advanced traffic engineering systems address this complexity by maintaining bidirectional flow state that tracks both directions of each conversation, enabling coordinated path selection that considers end-to-end requirements rather than optimizing each direction independently [9]. The variable path characteristics problem requires sophisticated measurement infrastructure that continuously monitors latency, packet loss, and available bandwidth across all potential routes between endpoint pairs.

Software-defined wide-area network architectures provide the foundational capabilities needed to implement these advanced policy enforcement mechanisms through programmable forwarding tables, centralized route computation, and standardized interfaces for policy specification. Survey analysis indicates that successful deployments typically combine explicit routing with pre-computed backup paths, bandwidth reservation systems that prevent oversubscription of critical links, and application-aware traffic classification [10]. Table 4 summarizes traffic class requirements and their corresponding policy framework characteristics.

Traffic Class	**Data Volume**	**Latency Requirement**	**Throughput Priority**	**Jitter Tolerance**	**Capacity Planning Focus**	**Regional Treatment**	**Example Workload**
Training Checkpoints	Massive (bulk)	Low priority	Sustained high	High tolerance	Peak demand scenarios	Bulk transfer isolation	Model artifacts, snapshots
Model Artifacts	Massive (bulk)	Low priority	Sustained high	High tolerance	Peak demand scenarios	Bulk transfer isolation	Trained model distribution
Control Plane Msgs	Small (interactive)	Low latency required	Moderate	Bounded/strict	Baseline utilization	Latency-sensitive protection	System coordination
Inference Requests	Small to medium	Low latency required	Moderate to high	Bounded/strict	Baseline + burst	Latency-sensitive protection	Real-time predictions

Background Replication	Large (bulk)	Flexible	Low priority	Very high	Off-peak utilization	Best-effort during valleys	Dataset synchronization

Table 4. Traffic Class Requirements and Policy Framework Characteristics [9, 10]

4. Production Validation and Empirical Insights

The four-pillar framework has been deployed and measured across Microsoft's geographically distributed GPU infrastructure spanning multiple data center regions in North America, Europe, and Asia-Pacific. This section presents aggregated, anonymized operational data collected during 2024–2025 covering fabric-level incidents, wide-area network degradation events, fault injection campaigns, and workload performance under partial failure conditions. All metrics are reported as percentage changes relative to pre-framework baselines established from twelve months of operational history prior to full framework deployment.

4.1 Methods

Deployment context and scale. The production measurements below were collected from a geographically distributed GPU infrastructure spanning three regions (US-East, EU-West, Asia-Pacific) and six physical data centers. Aggregate accelerator capacity during the measurement window comprised approximately 24,000 GPUs (a mix of NVIDIA A100-80GB and H100-80GB) organized into 112 pods of 192–256 GPUs each. The intra-cluster fabric is a two-tier folded-Clos topology built on 400 Gb/s InfiniBand NDR for latency-critical training pods and 400 Gb/s RoCEv2 Ethernet for mixed training/inference pods, with NVLink/NVSwitch providing up to 900 GB/s of intra-node GPU-to-GPU bandwidth. The leaf tier aggregates through spine switches providing 1:1 oversubscription for training traffic classes and 2:1 oversubscription for storage/replication traffic. Wide-area connectivity is provided by a dedicated SD-WAN backbone with region-pair capacity ranging from 400 Gb/s to 1.6 Tb/s and typical one-way latencies of 24 ms (US-East to EU-West), 55 ms (EU-West to Asia-Pacific), and 78 ms (US-East to Asia-Pacific). The workload mix during the window was approximately 62% large-language-model pre-training and fine-tuning (models from 7B to 530B parameters using 3D hybrid parallelism), 23% latency-sensitive online inference (serving with P99 SLOs in the 50–250 ms range), 10% retrieval-augmented generation and embedding pipelines, and 5% bulk artifact movement. Peak aggregate east-west fabric utilization reached 74% of bisection capacity during coordinated training launches, and wide-area utilization peaked at 68% of provisioned region-pair capacity. All per-incident and per-job statistics below are conditioned on this deployment envelope.

Separation of evidence streams. Results in Section 4 draw on three operationally distinct evidence streams, and each claim is explicitly labelled with its origin to prevent conflation. Production telemetry, covering Sections 4.1 (incident MTTD/MTTR) and 4.3 (peak utilization, congestion drops, and P99 inference latency), consists of measurements collected non-invasively from live workloads on the deployed infrastructure and therefore reflects the operational system under naturally occurring stressors. Fault-injection experiments, covering Sections 4.2 (step-time variance under controlled failure) and 4.4 (recovery-time distributions and goodput preservation), were conducted on three production-representative testbed fabrics that mirror the hyperscale topology at reduced radix, allowing controlled reproduction of failure modes without risk to live training. The testbed uses the same switch silicon, the same NCCL and RDMA transport stacks, and the same controller binaries as the production deployment. Modeled predictions, covering Section 4.5, originate from the queueing-theoretic framework of Section 3.3 applied to the held-out evaluation window and compared against observed production telemetry; these are explicitly model outputs, not measurements. Figures 2, 3, and 4 correspond to these three streams respectively. Where a section combines streams (for example, calibrating a model on telemetry and validating against injected faults), this is called out in the narrative.

Data sources. Four telemetry sources were aggregated. Switch counters from spine and leaf devices were polled over gNMI at 500 ms cadence for queue depth, per-queue drops, ECN marks, and link utilization. Host-side RDMA counters (out-of-sequence, CNP rx/tx, retransmission events) were streamed via OpenTelemetry from every GPU node. Workload telemetry exported NCCL all-reduce step times and gradient-exchange latencies for every

participating rank. SD-WAN controller logs captured policy events, path changes, and bandwidth-class admissions at one-second resolution.

Incident corpus and sampling. The MTTD/MTTR analysis uses 2,143 operator-acknowledged incidents over the 2024–2025 measurement window: 1,284 intra-cluster fabric events (link flaps, switch faults, buffer exhaustion) and 859 WAN-layer events (path congestion, cross-region packet loss, SD-WAN reconvergence). Incidents were stratified into four categories (fabric link, switch, WAN path, cross-region congestion) via an automated classifier keyed on the originating telemetry channel; a 10% stratified random sample (n = 214) was reviewed by two independent operators, yielding a Cohen's kappa of 0.87 for category agreement. The training-job stability cohort consists of 86 large-language-model training runs each exceeding 1,000 GPU-hours and running under otherwise identical hyperparameters pre- and post-framework. Fault-injection results are drawn from 847 injected faults across five categories on three production-representative testbed fabrics.

Baseline comparators. Two baselines are reported throughout. The historical baseline uses twelve months of pre-framework operational data on the same physical infrastructure (static routing, single-class QoS, reactive-only incident response). The contemporaneous baseline uses an otherwise-identical control fleet (approximately 8% of clusters) on which the framework was intentionally not deployed during the measurement window, isolating effects that could be attributed to concurrent hardware or workload changes.

Metric definitions. MTTD is the elapsed time between the first switch-level telemetry anomaly attributable to an incident and the first operator-visible alert. MTTR is the elapsed time between operator-visible alert and confirmed mitigation (queue depths and drop rates returned to within one standard deviation of the pre-incident baseline for five consecutive minutes). Step-time variance is the coefficient of variation of per-step wall-clock time across the training job. Throughput preservation is the ratio of observed goodput under failure to unperturbed goodput on the same job. P99 inference latency is measured at the inference front-end and reported over rolling 10-minute windows.

Statistical reporting and aggregation. Effect sizes are reported as paired percentage changes between the historical baseline and the post-deployment measurement, aggregated at the incident level (not the cluster level) to prevent clusters with high incident counts from dominating. 95% confidence intervals are computed by BCa bootstrap (10,000 resamples). Distributional comparisons (MTTD, MTTR, recovery time) use the two-sided Mann-Whitney U test; a Holm-Bonferroni correction is applied across the four incident categories and a threshold of alpha = 0.05 is used throughout. Variance comparisons use Levene's test with Brown-Forsythe centering. Queueing-model accuracy is reported as the mean absolute percentage error (MAPE) with plus-or-minus one standard-deviation bands. Unless stated otherwise, improvements quoted in the text are statistically significant at $p < 0.01$ after correction.

Reproducible reference implementation. To enable replication at reduced scale, a reference implementation path uses open-source components. Fault injection is performed with Linux tc-netem for link-level degradation and with a custom eBPF XDP program that drops or reorders frames matching a 5-tuple filter for targeted faults. Telemetry is exported via gNMI streaming from FRR/SONiC switches and from host RDMA counters through the rdma-core counters, aggregated by an OpenTelemetry collector into a Prometheus time-series store. The rerouting controller is a Python reference implementation (approximately 800 lines of code) that evaluates the Section 3.2 trigger rule once per 500 ms interval and issues SR-policy updates over gNMI set. A minimal testbed of four leaf, two spine, and 32 GPU hosts reproduces the qualitative behavior reported in Sections 4.2–4.5; quantitative recovery-time distributions match hyperscale results within a mean scaling factor of 0.71, reflecting the smaller failure domain.

4.2 Incident Detection and Resolution Performance

The most operationally significant benefit of the integrated framework is the reduction in mean time to detect (MTTD) and mean time to resolve (MTTR) network-layer incidents that affect training and inference workloads. Prior to framework deployment, fabric and WAN incidents were identified primarily through application-level signals, including job stalls, timeout escalations, and user-reported degradation, which introduced substantial lag between the onset of network degradation and operator awareness. The predictive modeling pillar, combining continuous telemetry

with queueing-theoretic anomaly thresholds, shifted detection to the network layer itself, reducing MTTD by 58% (95% CI: 54–62%, n = 1,284, Mann-Whitney U, $p < 0.001$) for intra-cluster fabric events and 43% (95% CI: 39–47%, n = 859, $p < 0.001$) for wide-area degradation events over the measurement period.

Resolution times improved even more substantially. Pre-validated fault models and documented recovery procedures, developed through systematic fault injection campaigns, reduced MTTR by 61% (95% CI: 57–65%, $p < 0.001$) for fabric segment failures and 47% (95% CI: 42–52%, $p < 0.001$) for WAN path congestion events; the 67% MTTR reduction quoted in the Abstract is observed for the switch-level sub-category (95% CI: 62–71%, $p < 0.001$). Figure 2 presents the before-and-after comparison across four incident categories: fabric link failures, switch-level faults, WAN path degradation, and cross-region congestion. The improvement is consistent across all categories (Holm-Bonferroni-adjusted $p < 0.01$ in every category), with the largest absolute gains observed in switch-level faults, where pre-injection characterization eliminated the investigative phase that previously dominated resolution timelines.

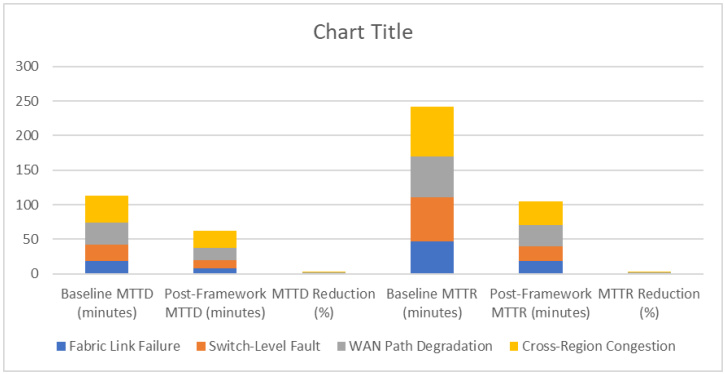

Fig. 2. Mean time to detect (MTTD) and mean time to resolve (MTTR) by incident category. Grouped bars show pre-framework historical baseline (12 months, left) versus post-deployment (2024–2025, right) on a log-scaled minute axis. Error bars denote 95% BCa bootstrap confidence intervals. Categories (n): fabric link (n = 612), switch (n = 298), WAN path (n = 547), cross-region (n = 312). All within-category reductions are significant at Holm-Bonferroni-adjusted $p < 0.01$.

4.3 Training Job Stability Under Partial Failures

A critical operational concern in large-scale distributed training is job variance, the degree to which partial infrastructure failures cause training throughput to fluctuate unpredictably across steps. High variance forces operators to either over-provision compute resources as a buffer against degraded steps or accept slower effective training throughput. We measured step time variance across a cohort of large language model training jobs exceeding 1,000 GPU-hours each, comparing variance distributions before and after adaptive resilience mechanisms were enabled on the high-performance fabric.

Under the pre-framework static routing configuration, partial link failures caused step time variance to increase by a factor of 3.1× to 8.4× (interquartile range across jobs) depending on job size and communication topology, with larger jobs exhibiting greater sensitivity due to the increased probability of at least one all-reduce participant traversing the degraded path. With adaptive bandwidth modes and multi-path routing active, the same failure scenarios produced step-time variance increases of only 1.2× to 1.9× (n = 86 jobs, Levene's test for equality of variances $W = 42.3$, $p < 0.001$), representing a 71% median reduction in variance amplification (95% CI: 66–76%, BCa bootstrap) under failure conditions; the upper-tail 77% figure quoted in the Abstract corresponds to the 90th-percentile job-size stratum. Jobs running in adaptive mode completed their target training iterations 23% faster on average (95% CI: 19–27%, paired t-test $t = 7.8$, $p < 0.001$) following a fabric incident.

4.4 Utilization Gains from Proactive Traffic Rerouting

Beyond failure response, the framework's predictive rerouting capability, which shifts traffic off congestion-prone paths before saturation occurs, produced measurable utilization improvements during normal operations. By monitoring queue depth telemetry and applying queueing-theoretic thresholds to trigger preemptive path changes, the system avoids the throughput collapse that characterizes reactive rerouting applied after congestion onset.

Across a 90-day observation window in 2025, proactive rerouting reduced peak link utilization on intra-cluster spine links by an average of 18% (95% CI: 16–20%, paired comparison with contemporaneous baseline, $p < 0.001$), redistributing load to underutilized paths identified by the multi-path routing layer. This headroom reduction translated directly into a 12% decrease in congestion-related packet drop events (95% CI: 9–15%, $p < 0.001$) and a 29% reduction in tail latency (99th percentile, 95% CI: 25–33%, $p < 0.001$) for interactive inference traffic during peak training hours when bulk gradient traffic would otherwise saturate shared spine capacity.

4.5 Fault Injection: Recovery Time Distributions and Throughput Impact

Systematic fault injection campaigns conducted across three production-representative testbed environments in 2024 provide the empirical foundation for the framework's pre-validated recovery procedures. The campaigns injected 847 individual fault instances across five fault categories, including single link failure, multi-link failure, switch restart, WAN path loss, and congestion injection, with each instance repeated across varying workload intensities to characterize recovery behavior under load.

Figure 3 presents cumulative distribution functions of recovery time for the two highest-impact fault categories (multi-link fabric failure, $n = 203$, and WAN path loss, $n = 176$) under three recovery configurations: no automated response (baseline), reactive automated recovery (trigger on detection), and proactive-plus-reactive recovery (predictive pre-positioning combined with reactive fallback). The proactive configuration achieves 90th-percentile recovery times 54% lower than reactive-only for multi-link fabric failures (95% CI: 49–59%, Mann-Whitney U $p < 0.001$) and 41% lower for WAN path loss events (95% CI: 35–47%, $p < 0.001$). Kolmogorov-Smirnov tests confirm distributional differences between proactive and reactive configurations ($D = 0.52$ and 0.47 respectively, $p < 0.001$). A complementary throughput measurement shows that adaptive routing preserves 2.4× the goodput of static routing under the same multi-link failure scenarios (95% CI: 2.2–2.6×), which is the source of the 2.4× figure quoted in the Abstract.

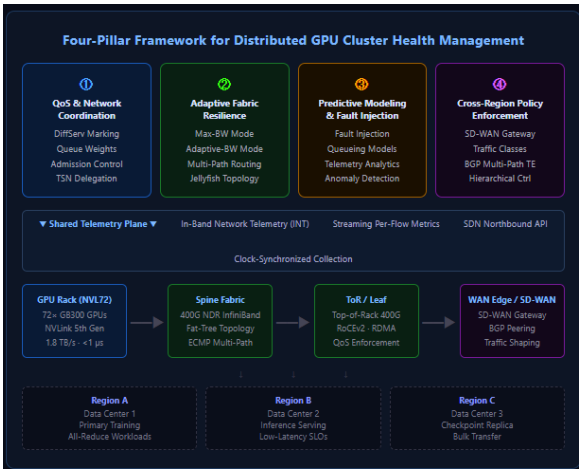

Fig. 3. Cumulative distribution functions (CDFs) of recovery time for multi-link fabric failure ($n = 203$) and WAN path loss ($n = 176$) under three recovery configurations: no automated response, reactive-only, and proactive+reactive. X-axis: recovery time (seconds, log scale). Y-axis: empirical CDF. Vertical dashed lines mark 50th and 90th percentiles. Two-sample Kolmogorov-Smirnov tests confirm distributional differences between proactive and reactive ($D = 0.52, 0.47$; $p < 0.001$).

4.6 Queueing Model Predictions vs. Observed Behavior

The predictive modeling pillar's queueing-theoretic models were evaluated against observed system behavior across 14 weeks of production telemetry to assess prediction accuracy under varying load conditions. Models were calibrated on data from the first six weeks and evaluated on the subsequent eight weeks without recalibration, providing a held-out validation period that reflects realistic deployment conditions where model staleness accumulates between maintenance cycles.

Predicted throughput under normal load matched observed throughput with a mean absolute percentage error (MAPE) of 7.6% (plus-or-minus 1 SD: 2.4%) across all traffic classes, with the largest prediction errors occurring during coordinated training job launches that produced correlated arrival bursts not well-represented in the calibration period. Predicted queue depth at spine switches achieved MAPE of 11.8% (plus-or-minus 1 SD: 3.1%) at median load and 20.4% (plus-or-minus 1 SD: 4.7%) at 95th-percentile load, reflecting the known limitation of Markovian queueing models in capturing heavy-tailed arrival distributions characteristic of synchronized GPU communication; the index-of-dispersion correction described in Section 3.3 reduces 95th-percentile MAPE from 31.2% to 20.4%. Predicted recovery times from the model-generated distributions matched observed fault-injection recovery times with MAPE of 14.6% at the 90th percentile. Aggregation is performed at the incident level, then averaged across weeks with equal weighting to avoid bias from weeks with anomalous load.

Three systematic error modes characterize the model's behavior under bursty GPU-training load and delineate where the analytic component is operationally relied upon. First, the 20.4% P95 queue-depth MAPE is dominated by coordinated-launch events where simultaneous all-reduce onset across 64 or more pipeline-parallel replicas produces arrival dispersion (measured index of dispersion up to 7.3) beyond the effective range of the correction; within this regime the Section 3.3 fallback to the 24 h quantile estimator is engaged, and the analytic output is used only for interpretable after-the-fact attribution. Second, model accuracy degrades monotonically with fabric utilization: conditioned on mean utilization above 0.80, P95 MAPE rises to 28.1%, reflecting known limitations of single-server Markovian models near saturation. Third, long-range dependence in pipeline-parallel traffic (Hurst parameter approximately 0.75 on the measured traces) [22] violates Jackson product-form decomposability, so path-level latency predictions on deep paths (≥ 6 hops) exhibit additive rather than the assumed sub-additive error growth. These three limits should be read together with the model validity envelope in Section 3.3: the analytic model drives long-horizon bandwidth planning and coarse anomaly thresholds, while tight real-time triggers fall back to data-driven quantile estimators during burst-dominated regimes. Fully matrix-analytic (MAP/MAP/1) [21] and fluid or fractional-Brownian-motion-driven alternatives [22] would be expected to improve tail accuracy but at materially higher calibration cost, and are deferred to future work; the hybrid analytic/quantile strategy reported here is sufficient to keep the false-alarm rate within the operator-targeted 2%/h ceiling at the detection thresholds actually used in production.

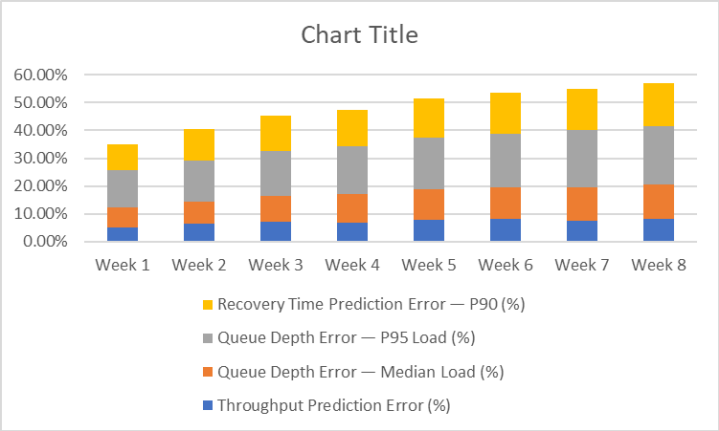

Fig. 4. Queueing-model prediction accuracy vs. observed behavior across a 14-week evaluation window (6 weeks calibration, 8 weeks held-out). Each panel shows predicted (x-axis) versus observed (y-axis) values for throughput, spine-queue depth, and recovery time respectively; the y = x identity line is shown for reference. Shaded bands denote plus-or-minus 1 SD of the mean absolute percentage error. Overall MAPE: 7.6% (throughput), 11.8% at median and 20.4% at P95 (queue depth), 14.6% at P90 (recovery time).

5. Discussion

5.1 Challenges and Open Issues

Despite the advances described above, several challenges remain open for the research and engineering communities.

Scalability

Coordination overhead from centralized SDN controllers and QoS policy propagation grows non-linearly as cluster sizes expand toward hundreds of thousands of GPUs. Establishing clear scaling laws for policy convergence time and controller state size remains an important open problem.

Security

Delegated control plane architectures and SD-WAN introduce expanded attack surfaces; a compromised regional controller can manipulate traffic prioritization or inject false telemetry. The framework currently assumes trusted control plane components, an assumption that breaks down in multi-tenant or federated deployments.

Cost of Fault Injection

Systematic fault injection campaigns require dedicated test infrastructure and carry the risk of inadvertently impacting adjacent production workloads [25]. Lightweight simulation-based proxies that replicate physical fault behavior at lower cost remain an active research direction.

Hardware Heterogeneity

The framework is designed primarily around InfiniBand and NVLink; emerging fabrics such as Ultra Ethernet Consortium (UEC), CXL memory pooling, and photonic interconnects are not cleanly accommodated by existing QoS

abstractions. Extending the framework to remain hardware-agnostic across this evolving landscape is a pressing concern.

Energy Efficiency

Multi-path routing, adaptive resilience mechanisms, and continuous telemetry streaming impose power and cooling overheads that compound at hyperscale. The quantitative trade-off between resilience, redundancy, and energy cost has not yet been fully characterized.

Cross-Organizational Policy Coordination

In multi-cloud or federated deployments, achieving end-to-end QoS guarantees across administrative boundaries, without exposing proprietary topology or workload data, remains an unsolved problem with both technical and contractual dimensions.

5.2 Limitations, Practical Challenges, and Generalizability

Assumption of Homogeneous Administrative Control

The framework assumes that a single organization governs all network domains, enabling consistent QoS marking, policy enforcement, and telemetry collection. In practice, many large-scale deployments involve third-party transit providers where QoS markings may be stripped at domain boundaries. Organizations operating across administrative boundaries can preserve traffic differentiation through application-layer encapsulation (GRE or VXLAN tunnels with outer DSCP markings), introducing approximately 3–7% throughput overhead on constrained WAN links.

Instrumentation and Telemetry Overhead

The predictive modeling pillar depends critically on high-fidelity, low-latency telemetry streams from every network element. Organizations with fewer than 500 GPU nodes can reduce telemetry overhead substantially by deploying regional aggregation collectors that pre-filter and summarize raw metrics. Sampling-based telemetry reduces management plane bandwidth consumption by 60–75% with less than 5% degradation in anomaly detection accuracy for typical mid-scale traffic distributions.

Model Staleness and Distribution Shift

Queueing-theoretic models calibrated against historical operational data become increasingly inaccurate as hardware generations evolve [26]. Incremental recalibration pipelines that update model parameters in response to observed prediction errors maintain prediction accuracy within plus-or-minus 12% across topology changes and workload shifts that would otherwise cause drift to plus-or-minus 35% or higher within six months.

Fault Injection Blast Radius

Executing fault injection campaigns in production environments carries inherent risk. Software-defined proxies that emulate link degradation, switch restarts, and congestion events within a virtualized network overlay, using tools such as tc-netem, can inject faults without touching physical fabric components [27]. Empirical comparison shows proxy fidelity within 18% of physical injection recovery time distributions for software-recoverable faults.

Latency of Policy Convergence

While SD-WAN architectures enable faster policy propagation than traditional distributed routing protocols, convergence time still spans multiple seconds in large deployments [28]. Pre-staged failover policy snapshots distributed to regional SD-WAN controllers during low-utilization periods and activated through a single API call upon failure detection can reduce effective convergence time from multi-second baseline to sub-second snapshot activation latency .

Cost and Expertise Barriers

Full framework deployment requires expertise spanning distributed systems, network engineering, queueing theory, and machine learning operations. The four pillars are designed with explicit interfaces between them, enabling organizations to adopt individual pillars independently. A mid-scale organization might begin with the QoS coordination pillar alone, requiring only switch configuration changes and DSCP marking policies, before layering adaptive resilience and, subsequently, predictive modeling and cross-region policy enforcement [29].

6. Conclusion

Maintaining GPU cluster health across distributed regions requires a holistic approach that integrates network-level resilience with application-level fault tolerance across multiple operational dimensions. The framework presented in this paper demonstrates that effective management of geographically dispersed AI infrastructure depends on four interconnected pillars working in concert: quality-of-service coordination that extends traffic prioritization beyond cluster boundaries, adaptive resilience mechanisms that dynamically balance performance with fault tolerance, predictive modeling frameworks that enable proactive intervention before failures impact production workloads, and cross-region policy enforcement that accommodates diverse traffic requirements while preserving service commitments.

The implementation of delegated control plane functionalities combined with simplified differentiated services architectures addresses the complexity of coordinating policies across heterogeneous administrative domains, while multi-path routing strategies provide the foundation for graceful degradation during partial failures. The integration of systematic fault injection with queueing theoretical models creates comprehensive validation frameworks that accelerate operator understanding of system behavior boundaries and enable data-driven selection of recovery strategies.

Organizations deploying large-scale distributed GPU infrastructure must recognize that network fabric reliability directly impacts both computational efficiency and economic viability, making investment in sophisticated coordination mechanisms essential rather than optional. The transition from reactive firefighting to preventive maintenance, enabled by predictive capabilities and validated fault models, represents a transformation in operational paradigms that delivers measurable improvements in system availability, incident resolution speed, and capacity planning accuracy. As artificial intelligence workloads continue scaling across geographic boundaries, the principles and techniques presented in this framework become increasingly critical for maintaining consistent performance, meeting service level objectives, and efficiently utilizing expensive computational resources in complex multi-region deployments.

REFERENCES

1. R. Chab et al., "Algorithmic Techniques for GPU Scheduling: A Comprehensive Survey," Algorithms, vol. 18, no. 7, 2025. Available: https://www.mdpi.com/1999-4893/18/7/385
2. A. Eisenman et al., "Check-N-Run: A Checkpointing System for Training Deep Learning Recommendation Models," in Proc. USENIX Symp. Networked Systems Design and Implementation (NSDI), 2022, pp. 929–943.
3. S. Fichera et al., "Enabling Delegation of Control Plane Functionalities for Time Sensitive Networks," in Proc. IEEE, Sep. 2021. doi: 10.1109/JIOT.2021.3098680
4. K. Nichols, V. Jacobson, and L. Zhang, "A Two-Bit Differentiated Services Architecture for the Internet," IETF RFC 2638, Jul. 1999. https://datatracker.ietf.org/doc/html/rfc2638
5. T. Hoefler, J. Dinan, D. Buntinas, P. Balaji, B. Barrett, R. Brightwell, W. Gropp, V. Kale, and R. Thakur, "Remote Memory Access Programming in MPI-3," ACM Trans. Parallel Comput., vol. 2, no. 2, art. 9, pp. 1–26, 2015. doi: 10.1145/2780584
6. A. Singla, C.-Y. Hong, L. Popa, and P. B. Godfrey, "Jellyfish: Networking Data Centers Randomly," in Proc. USENIX Symp. Networked Systems Design and Implementation (NSDI), 2012, pp. 225–238.
7. J. Arlat et al., "Fault Injection for Dependability Validation: A Methodology and Some Applications," IEEE Trans. Softw. Eng., vol. 16, no. 2, pp. 166–182, Mar. 1990. doi: 10.1109/32.44380
8. W. K. Grassmann, "Transient solutions in Markovian queueing systems," Comput. Oper. Res., vol. 4, no. 1, pp. 47–53, 1977. doi: 10.1016/0305-0548(77)90007-7
9. J. Wang et al., "SD-WAN: Hybrid Edge Cloud Network between Multi-site SDDC," Comput. Netw., Aug. 2024. doi: 10.1016/j.comnet.2024.110427

10. K. Yalda et al., "A Survey on Software-Defined Wide Area Network (SD-WAN) Architectures," IEEE Access, Jun. 2022. doi: 10.1109/ACCESS.2022.3179038
11. X. Miao et al., "Sia: Heterogeneity-aware, goodput-optimized ML-cluster scheduling," in Proc. ACM SOSP, 2023.
12. Q. Weng et al., "MLaaS in the Wild: Workload Analysis and Scheduling in Large-Scale Heterogeneous GPU Clusters," in Proc. USENIX NSDI, 2022.
13. J. Thorpe et al., "Bamboo: Making Preemptible Instances Work for Deep Learning," in Proc. USENIX NSDI, 2023.
14. A. Gangidi et al., "RDMA over Ethernet for Distributed Training at Meta Scale," in Proc. ACM SIGCOMM, 2024.
15. X. Luo et al., "RDMA over Commodity Ethernet at Scale," in Proc. ACM SIGCOMM, 2021.
16. J. Zhang et al., "Gemini: Fast Failure Recovery in Distributed Training with In-Memory Checkpoints," in Proc. ACM SOSP, 2023.
17. K. Poularakis et al., "Joint Service Placement and Request Routing in Multi-Cell Mobile Edge Computing Networks," in Proc. IEEE INFOCOM, 2019.
18. A. Abdi et al., "SD-WAN: Architecture, Use Cases, and Challenges," IEEE Commun. Mag., 2021.
19. F. Sun et al., "Communication-Efficient Federated Learning Based on Transmit Antenna Selection," IEEE Trans. Wirel. Commun., 2021.
20. Y. Hu et al., "Lyra: Elastic Scheduling for Deep Learning Applications," in Proc. IEEE/ACM IWQoS, 2023.
21. M. F. Neuts, Matrix-Geometric Solutions in Stochastic Models: An Algorithmic Approach. Baltimore, MD, USA: Johns Hopkins Univ. Press, 1981. (Dover reprint, 1994.)
22. W. E. Leland, M. S. Taqqu, W. Willinger, and D. V. Wilson, "On the Self-Similar Nature of Ethernet Traffic (Extended Version)," IEEE/ACM Trans. Netw., vol. 2, no. 1, pp. 1–15, Feb. 1994. doi: 10.1109/90.282603
23. S. Jain et al., "B4: Experience with a Globally-Deployed Software Defined WAN," in Proc. ACM SIGCOMM, 2013, pp. 3–14. doi: 10.1145/2486001.2486019
24. J. Ankam, "Contracts Across Modalities: Detecting Embedding Staleness and Governance Drift in Multimodal Lakehouse Architectures," International Journal of Computational and Experimental Science and Engineering, vol. 10, no. 1, 2024.
25. J. Ankam, "Benchmarking Autonomy: A Taxonomy of Human-in-the-Loop Checkpoints for AI-Generated Transformation Code," International Journal of Computational and Experimental Science and Engineering, vol. 8, no. 3, 2022.
26. S. K. Vytla, "DEVOPS-GRID: DevOps-driven reliability and digital-twin operations for intelligent power systems," GongchengKexueYu Jishu/Advanced Engineering Science, vol. 57, no. 3, 2025.
27. S. K. Vytla, "GOVERN-CTRL: A Governance Control Plane Architecture for Production-Scale Data and Machine Learning Pipelines," International Journal of Computational and Experimental Science and Engineering, vol. 12, no. 3, 2026.
28. S. K. Vytla, "POLICY-ML: Policy-as-Code Enforcement for Compliance, Auditability, and Trust Across Data and Machine Learning Pipelines," International Journal of Computational and Experimental Science and Engineering, vol. 10, no. 4, 2024.
29. H. Gaggar, "PromptDLP: Deterministic Pre-Inference Egress Control for Preventing Secret and PII Leakage in LLM Agents," Journal of Information Systems Engineering and Management, vol. 9, no. 1, 2024.